Pyrene-functionalized tungsten disulfide as stable resistive photosensor

Ruben Canton-Vitoria, Sebastian Nufer, Xiaoyang Che, Yuman Sayed-Ahmad-Baraza, Raul Arenal, Carla Bittencourt, Adam Brunton, Alan Dalton, Christopher Ewels, Nikos Tagmatarchis

Pyrene-functionalized tungsten disulfide as stable resistive photosensor

Ruben Canton-Vitoria,[a¶] Sebastian Nufer [b, c] Xiaoyang Che [d,e], Yuman Sayed-Ahmad Baraza,[d] Raul Arenal,[f,g,h] Carla Bittencourt,[i] Adam Brunton,[b] Alan B. Dalton,[c] Christopher P. Ewels,[d] Nikos Tagmatarchis[a]**

[a] Theoretical and Physical Chemistry Institute, National Hellenic Research Foundation, 48 Vassileos Constantinou Avenue, 116 35 Athens, Greece.

[b] M-Solv Ltd, Oxonian Park, Langford Locks, Kidlington, Oxford, OX5 1FP, United Kingdom.

[c] Department of Physics, University of Sussex, Brighton, BN1 9R, United Kingdom.

[d] Institut des Materiaux Jean Rouxel (IMN), UMR6502 CNRS, Universite de Nantes 2 Rue de la Houssiniere, BP32229, 44322 Nantes, France.

[e] Centre de Recherche Paul Pascal (CRPP)-UMR5031, 115 Avenue du Dr. Albert Schweitzer, 33600 Pessac, France.

[f] Laboratorio de Microscopias Avanzadas, Instituto de Nanosciencia de Aragon, Universidad de Zaragaza, 50018 Zaragoza, Spain.

[g] ARAID Foundation, 50018 Zaragoza, Spain.

[h] Instituto de Ciencias de Materiales Aragón, CSIC-U. Zaragoza, 50009 Zaragoza, Spain.

[i] Chimie des Interactions Plasma-Surface, University of Mons, 20 Place du Parc, 7000 Mons, Belgium.

KEYWORDS: transition metal dichalcogenides, pyrene, functionalization, photosensor

ABSTRACT. Pyrene carrying an 1,2-dithiolane linker was employed to functionalize exfoliated WS_2 and the resulting material used in a proof-of-concept application as a photoresistor type sensor. The WS_2-pyrene hybrid material was comprehensively characterized by spectroscopic, thermal and microscopy techniques, coupled to density functional theory modelling. The high solubility of the WS_2-pyrene hybrid material allows easy manipulation in wet media, making it suitable for device fabrication. Thus, a two-terminal resistive photosensor was developed and tested for photodetection. The photosensitivity of WS_2 was improved by the presence of covalently attached pyrene by a factor of 2-3, the response linearly dependent on light intensity. Device reaction time was also improved, and critically the photosensor stability was significantly enhanced. Functionalization of exfoliated WS_2 material heals vacancies, oxidation and other damage sites liable to impede photoelectric response. This proof-of-concept study opens the way for incorporation of diverse chromophores active in the visible and/or NIR region of the electromagnetic spectrum to WS_2 in order to stabilise it and broaden its photoresistive sensing applicability.

INTRODUCTION

The combination of high area-to-volume ratio with band gaps in the visible region makes transition metal dichalcogenides (TMDs) attractive for energy and sensing applications.[1-4] Depending on the process used, exfoliation of tungsten disulfide WS_2 gives either semiconducting or metallic nanosheets.[5-10] Functionalizing these improves their marginal dispersibility in wet media, and can additionally impart new functionality. For example, WS_2 nanosheets functionalized with positively charged ammonium moieties have been used to electrostatically couple to negatively charged photoactive species such as derivatized porphyrins,[11] carbon nanodots[12] and a water-soluble polythiophene.[13] In these cases, functionalization is achieved through addition of 1,2-dithiolanes to exfoliated WS_2, rationalized by the high binding affinity of sulfur for tungsten atoms. Precisely, 1,2-dithiolanes efficiently bind at the edges of WS_2 layers, where sulfur vacant sites are numerous in comparison with those in the basal plane. A similar methodology has also been employed to directly incorporate pyrene,[14] carbon nanodots,[15] phthalocyanine[16] and porphyrin[17] species onto TMDs via robust and stable bond formation. The resulting electron donor-acceptor hybrid systems are important in electrocatalytic processes and photoinduced charge-transfer phenomena.

Semiconductor resistive photosensors operate through a reduction of electrical resistance under illumination, with light whose energy is close to the semiconductor band gap. Key requirements are high surface area, sub-nanometric thickness, and a controllable band gap within the solar irradiation region. TMDs are candidates for nanoscale photosensing, potentially replacing silicon and other materials.[18] Amongst these, nanosized WS_2 shows the fastest light-response[19-21] and has excellent carrier mobility, high photoelectrical on/off ratio and stability, with excitons in the visible region of the electromagnetic spectrum.[22-26] However, stability of TMDs over time is a limiting factor.[27, 28] Thus, improving the WS_2 sensitivity, sig-

nal/noise, response time and stability is strongly desired for real sensing applications.

Heterostructures based in WS_2 with e.g. graphene, show excellent results, sharply enhancing sensitivity, however, their realization requires tedious engineering technology with individual design of electrodes, handicapping any scalable production.[29] On the other hand, functionalization of 2D nanostructures allows the realization of material in bulk quantities with robust properties, suitable for technological applications. Focusing on the development of light sensors, functionalization of WS_2 with Au nanospheres strongly enhanced the sensitivity of CVD grown WS_2 at 590 nm and 740 nm, however with a slow speed response of 3s.[30] Functionalization with carbon nanotubes improved the response up to 0.003μs at 633 and 875 nm, and in addition, resulted in fourfold enhancement of the photo-response.[31] Incorporation of polyimide into WS_2 resulted in flexible devices with 10-fold sensitivity increase and a fast response of 500μs.[32.] An excellent enhancement of photo-response (1000× at 532 nm) was also found upon interfacing WS_2 with graphene oxide nanoparticles, however, the noise/response enhanced proportionally, and response time decreased around 10 times.[33] Functionalization of WS_2 with nanocrystals of SnSe enhanced the photo-response ratio to the NIR (1062 nm) and the sensitivity by 1 or 2 orders of magnitude, however, the fast response decreased to half.[34] Functionalization of WS_2 with black phosphorous nanosheets[35] improved the photo-response, however, with the disadvantage of decreasing the fast response. Overall, despite some studies shown enhancement of the stability after functionalization, lack of reference WS_2 makes difficult to draw reliable conclusions on thermal, electronic or chemical stability.

Photosensing evaluation of hybrid materials featuring organic dyes covalently incorporated on WS_2 that participate in light-induced photophysical events has yet to be performed. Herein, we report on the functionalization of exfoliated WS_2 with a pyrene modified 1,2-dithiolane derivative, followed by assessment of the resultant hybrid material as a stable resistive photosensor. We develop an easy and scalable two-terminal resistive photosensor with the pyrene-modified WS_2 and find photoinduced sensitivity enhancement from the pyrene species to the conduction band of WS_2. In addition, the WS_2-pyrene based prototype device shows long term stability, rationalized by considering healing of defective sulfur sites by the covalent 1,2-dithiolane addition. The current study provides valuable information related to the electronic character of the hybrid material, understanding its resistive photosensing behavior and will allow systematic exploitation of its capabilities.

RESULTS AND DISCUSSION

Bulk WS_2 was exfoliated to semiconducting nanosheets through chlorosulfonic acid treatment following an experimental procedure developed in our labs.[5] The general scheme for the functionalization process is illustrated in Figure 1. In a typical reaction, treatment of exfoliated WS_2 with an excess of 1,2-dithiolane derivative **1** produces pyrene-modified WS_2-based hybrid material **2**. Filtration over PTFE membrane (0.1 μm pore size), followed by washing with dichloromethane, ensured that **2** was free from organic impurities and guaranteed the absence of any physisorbed pyrene species. Hybrid material **2** forms stable dispersions in DMF and methanol without significant precipitation (even for several months). The dispersibility of **2** in those solvents allows easier manipulation and processing e.g. fabrication of devices by drop-casting processes *en route* the development of active electrodes. The molar absorptivity of hybrid **2** in DMF was found to be 434 L g^{-1} m^{-1} at 480 nm. In contrast, the dispersibility of **2** in solvents such as o-DCB, THF and dichloromethane was marginal.

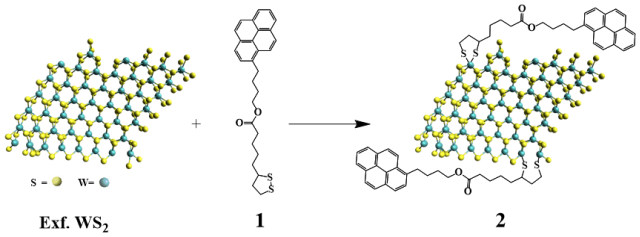

Figure 1. Functionalization of exfoliated WS_2 with pyrene 1,2-dithiolane derivative **1** forming WS_2-pyrene hybrid material **2**.

Attenuated-total-reflectance infra-red (ATR-IR) spectroscopy confirms the successful functionalization. Briefly, vibrations due to the presence of the carbonyl ester moiety at 1730 cm^{-1} and strong C-H stretching vibrations at 2950 cm^{-1} were identified for hybrid material **2** (Figure 2a). Similar IR vibrations were found in the spectrum of 1,2-dithiolane derivative **1**. Thermogravimetric analysis (TGA) allows estimating the degree of functionalization in hybrid material **2**. Exfoliated WS_2 is thermally stable up to at least 800 °C under nitrogen atmosphere. However, **2** showed a mass loss of 4.4 % in the temperature range 250-550 °C (Figure 2b), associated with thermal decomposition of the organic moieties covalently anchored on WS_2. This mass loss corresponds to one pyrene unit for every 41 WS_2 units within hybrid material **2**.

Resonant Raman spectra were obtained upon excitation at 514 nm. In both exfoliated WS_2 and hybrid material **2**, modes due to the 2LA(M), E^1_{2g}, and A_{1g} are visible at 350, 354 and 419 cm^{-1}, respectively. However, the intensity of the defective mode 2LA(M) is significantly reduced for hybrid material **2** compared to exfoliated WS_2 (Figure 2c), suggesting that defects are reduced as functionalization occurs at sulfur-defect sites.

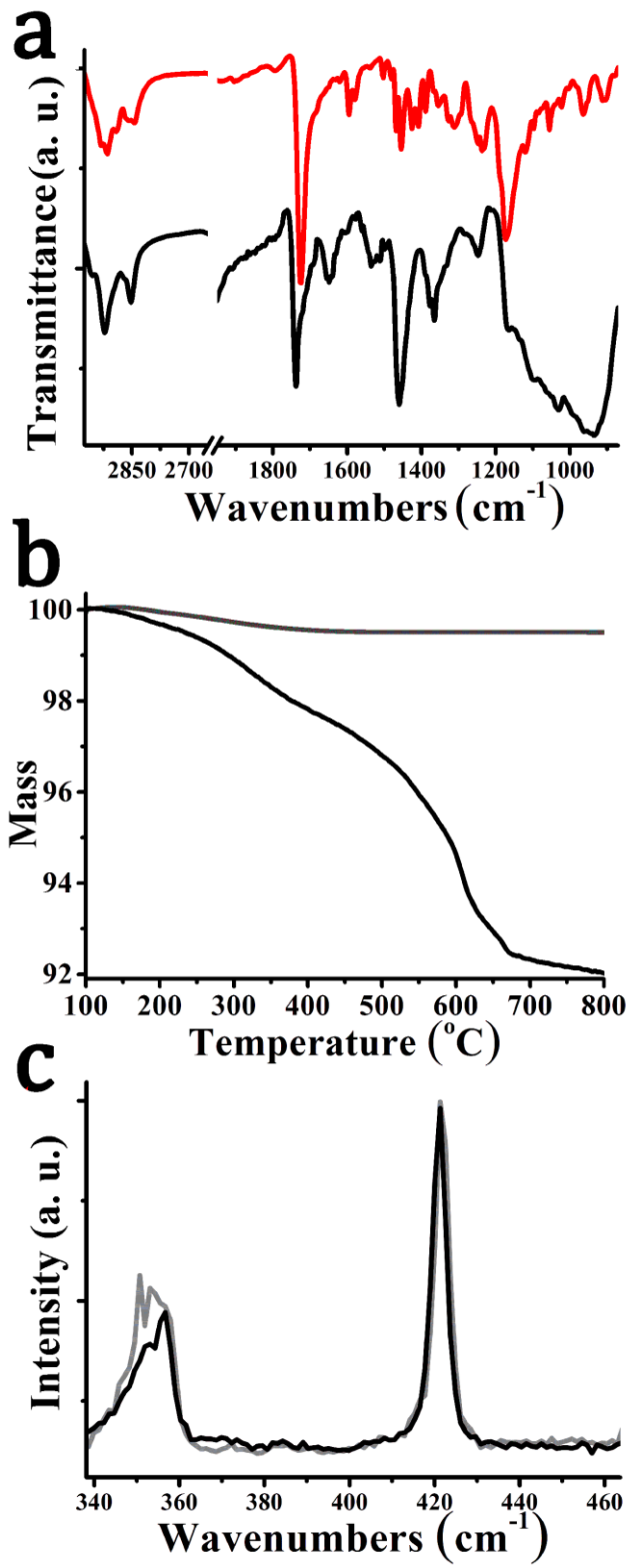

Figure 2. (a) Thermographs for exfoliated WS_2 (gray) and hybrid material **2** (black), obtained under nitrogen atmosphere. (b) ATR-IR spectra for pyrene derivative **1** (red) and hybrid material **2** (black). (c) Raman spectra for exfoliated WS_2 (gray) and hybrid material **2** (black), obtained upon 514 nm excitation.

This can be further explored using X-ray photoelectron spectroscopy (XPS) of the W*4f* and S*2p* XPS core level spectra (Figure 3). The energy positions of the doublet components S $2p_{3/2}$ and S $2p_{1/2}$ at 163.7 and 162.5 eV, respectively, and of W $f_{5/2}$ and W $f_{7/2}$ at 35.1 and 32.9 eV, respectively, indicate a W valence of +4 and a pure hexagonal phase of exfoliated WS_2. The atomic ratio S/W estimated for exfoliated WS_2 and pyrene modified WS_2 hybrid material **2** is 1.75 and 1.95 (Figure 3), i.e. corresponding to non-stoichiometric surface concentrations of $WS_{1.75}$ and $WS_{1.95}$, respectively. This demonstrates that sulfur vacancies are created during the exfoliation process, which are 'reduced' upon functionalization with pyrene derivative **1** via interactions of the 1,2-dithiolane unit with the sulfur vacant sites. This WS_2 restoration process during functionalization is also seen in an XPS doublet at 38.3 eV and 36.1 eV corresponding to residual WO_3. After functionalization, the relative intensity of this doublet decreases from 4% to 2% of the total W 4*f* core level and shifts 0.2 eV towards low binding energy. Such shift is in concordance with other chromophores functionalized TMDs, and it is related with charge transfer interaction between the surface assembled chromophores and WS_2.[36]

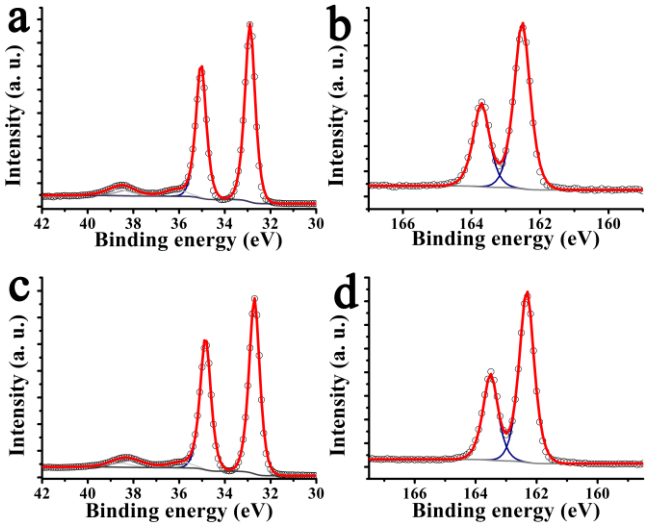

Figure 3. The W *4f* core levels of (a) exfoliated WS_2, and (c) WS_2-pyrene hybrid **2**, reproduced using a component at 38.7 eV generated by photoelectrons emitted from W $5p_{3/2}$ in WS_2 and two doublets W $f_{5/2}$ and W $f_{7/2}$, a high intensity one (35.1 eV and 32.9 eV) belonging to hexagonal WS_2 and a low intensity one (38.3 eV and 36.1 eV) to WO_3. The S 2*p* core levels are composed of a doublet (S $2p_{3/2}$ and S $2p_{1/2}$) at (b) 163.7 eV for exfoliated WS_2, and (d) 162.5 eV for WS_2-pyrene hybrid material **2**.

The stoichiometry change proposed by XPS corresponds to a higher functionalization degree than suggested from the TGA data. Since XPS is highly surface sensitive, this suggests that the material is not monolayer but contains also multi-layer flakes and particles. This is confirmed via high-resolution scanning TEM (Figure 4a-c), where it can be seen that typical material indeed contains multi-layer flakes. This can actually be an advantage in terms of improved optical absorption for photoresistivity, as discussed further below. Electron energy-loss spectroscopy (EELS) confirms that pyrene is present ubiquitously across the flakes, see Figure 4c. An EELS spectrum-line (SPLI) has been collected following the green marked line (Figure 4c). Three different EEL spectra (marked as (i) to (iii)) have been selected from this SPLI and are displayed in Figure 4d. S-$L_{3,2}$ edge from WS_2 can be observed in the three spectra. In the red EEL spectrum (ii), the C-K edge

associated to pyrene is visible. From the analysis of the fine structures near of the edge (ELNES), this C-K edge is clearly different to this one from amorphous carbon,[37-39] confirming the presence of pyrene.

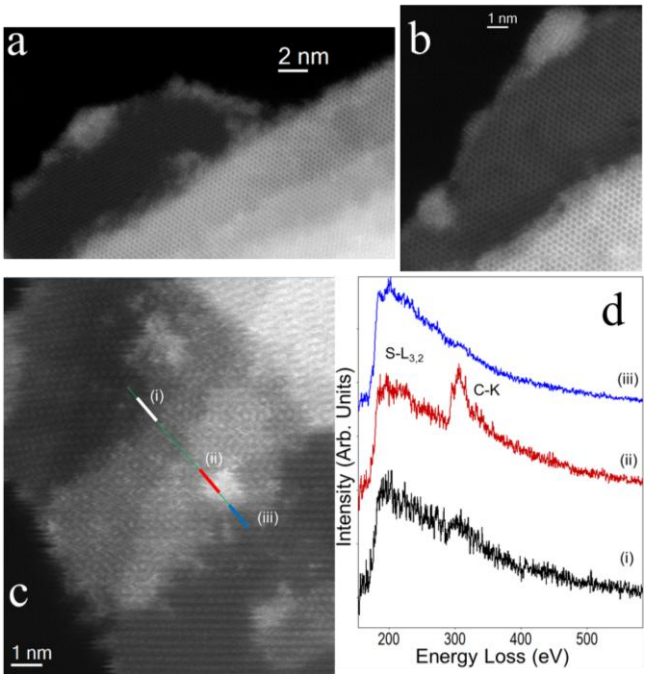

Figure 4. (a-c) High-angle annular dark-field (HAADF) high-resolution scanning transmission electron micrographs of typical WS_2-pyrene hybrid **2**. (c) An EELS SPLI has been collected following the green line marked in this HAADF image. (d) Three EEL spectra corresponding each of them to the sum of four EEL spectra collected in each of these highlighted areas (i)-(iii) are depicted in Fig. 4d. See text for more details.

We turn next to the optical response of the material. The electronic absorption spectrum of hybrid material **2** is governed by characteristic bands attributed to the semiconducting phase of WS_2, namely, the A excitonic band centered at 645 nm, the indirect excitonic B band at 545 nm, and two optical transitions associated with the density of states at 480 and 420 nm. Additional bands directly derived from the optical absorption of pyrene in hybrid material **2** are also discernable at 325 and 340 nm (Figure 5a). In general, the UV-Vis spectrum of **2** is a simple superimposition of the absorption spectra of exfoliated WS_2 and pyrene derivative **1**, implying marginal, if any, electronic interactions between the two species at the ground state. However, the presence of pyrene moieties in hybrid material **2** guarantees more efficient absorption in the visible region in comparison with exfoliated WS_2, suggesting an improvement of the response when employed as photo-resistive sensor (see below).

In sharp contrast, intimate electronic communication between pyrene and WS_2 is visible in **2** at the excited state upon photoillumination at 340 nm. Specifically, based on steady-state photoluminescence assays, the characteristic emission bands of pyrene in derivative **1**, centered at 375 and 395 nm, were substantially quenched by WS_2 in hybrid material **2** (Figure 5b), for samples possessing equal optical concentration at the excitation wavelength. This is to say that intra-hybrid transduction of energy from the singlet excited state of pyrene to WS_2 takes place in **2**. It should be noted that the broad feature at 490 nm observed in the photoluminescence spectrum of **2** is due to the pyrene excimer and should not be confused with impurity or WS_2 exciton features. In fact, excimer formation in hybrid **2** can be considered as an additional electronic interaction between WS_2 and pyrene, probably due to a favorable molecular orientation of pyrene onto the WS_2 nanosheets.

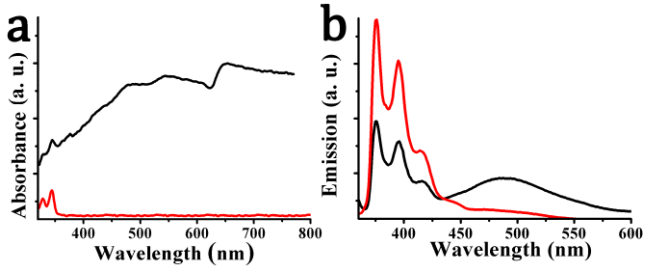

Figure 5. (a) UV-Vis spectra and (b) photoluminescence spectra (λ_{exc} 340 nm), for pyrene derivative **1** (red) and hybrid material **2** (black), obtained in DMF.

These interactions can be explored further via density functional theory (DFT) calculations of pyrene over the surface of WS_2. The calculations show strong binding (81.2 Kcal/mol) to the surface, with the pyrene only stable in a surface-parallel configuration (other orientations relaxing spontaneously to the parallel case, see Supplementary Movie M1). The projected density of electronic states (PDOS) shows strong interaction between monolayer WS_2 and pyrene (Figure 6a). In comparison to isolated pyrene (Figure 6b), the hybrid system shows an upshift in pyrene electronic states. Additionally, while the highest occupied molecular orbital (HOMO) remains sharp and localized, there is a strong broadening of the pyrene lowest-occupied molecular orbital (LUMO) and LUMO+1 states, where they couple strongly with electronic states in the neighbouring WS_2 (Figure 6a). This strong coupling confirms that HOMO→LUMO and HOMO→(LUMO+1) excitations in the pyrene will rapidly transfer to the conduction band of the underlying WS_2, resulting in the observed quenching of the emission bands of pyrene. Given the difference in electronic behavior of mono- and multi-layer WS_2[40] we also calculated the PDOS for pyrene on bilayer WS_2 (Supporting Information, Figure S1), where similar coupling is once again observed.

Figure 6. Calculated projected density of electronic states for (a) monolayer-WS_2 and pyrene at infinite separation, (b) Pyrene on monolayer WS_2 surface in ground state and energies are shifted to place the Fermi level at 0 eV in each case, states localized on W/S/pyrene are marked in red/green/blue, respectively.

In order to understand further the phenomena occurring at the excited states, time-resolved photoluminescence assays were performed and the fluorescence lifetime based on the time-correlated-single-photon-counting method was determined. The emission decay of pyrene derivative **1** could be mono-exponentially fitted with a long lifetime of 3.78 ns (Supporting Information, Figure S2). However, the emission decay of hybrid material **2** consists of two components with lifetimes of 0.22 and 3.79 ns. The fast 0.22 ns component is assigned to charge and/or energy transfer from pyrene to WS_2 in accordance with the steady-state photoluminescence quenching results, and is consistent with the strong coupling observed in the DFT results. Based on equations (1) and (2), the quenching rate constant k^S_q for the singlet excited state of **2**

was evaluated as 4.28×10^{-9} s^{-1} and its quantum yield Φ^{S}_{q} was calculated to be 0.94.

$$(1): \quad k_q^s = \frac{\tau_o - \tau_f}{\tau_o \tau_f}$$

$$(2): \Phi_q^s = k_q^s \tau_f$$

where τ_f refers to the lifetime of the fast-decaying component in **2**, and τ_o refers to the lifetime of free pyrene **1**.

Next, WS_2-pyrene hybrid material **2** was tested as a resistive photosensor and compared to pristine WS_2. The sensor consists of 700nm-thick metallic Molybdenum interdigitated electrodes on a glass substrate (~100cm^2), with exfoliated WS_2 or WS_2-pyrene material **2** drop-cast and confined using transparent Scotch tape (full details are given in the Supporting Information). Figure 7 shows the resistance response of the photosensor to white light irradiation.

Pristine WS_2 shows a small resistance change caused by photoexcitation of carriers in the semiconductor, which is weakly proportional to the light intensity (Figure 7a). Sample resistance increases gradually over time and additionally the device shows significant drift, which is clearer in exposure measurements taken over several minutes (Figure 7b). Both of these effects can be ascribed to thermal and photoinduced oxidation. Considering next the WS_2-pyrene hybrid material **2** under light irradiation, electron transfer additionally occurs from pyrene to the semiconducting WS_2 nanosheets, shifting the Fermi level and decreasing the device resistance. This can be seen in Figure 7a where the resistance response is enhanced by typically 2-3 times over that of exfoliated WS_2. In this case, the resistance drop is strongly proportional to light intensity. Additionally, in this case the device maintains a stable baseline during and after long-time exposure pulse (Figure 7b) and shows reproducible sensitivities at equivalent pulse measurements (Supporting Information, Figure S3). Finally, the rapid response for hybrid material **2** was 710ms and the recovery time was 725ms at 6400mW/cm^2 which unlike most literature functionalised WS_2 sensors is 5 and 15 ms faster compared to untreated exfoliated WS_2, respectively (Supporting Information, Figure S4). This small but quantifiable improvement in **2** suggests a decrease of photo-reduction trapping holes correlated with a decrease of the number of sulfur defects upon the 1,2-dithiolane functionalization with pyrene derivative **1**.

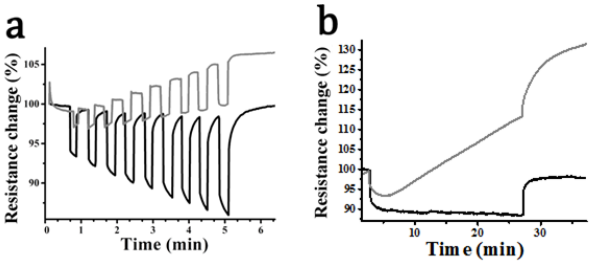

Figure 7. Resistance response of hybrid material **2** (black) and exfoliated WS_2 (gray) with (a) increasing light irradiation from 400 to 1200 mW/cm^2, and (b) continuous light irradiation with an intensity of 600 mW/cm^2 showing baseline drift in the exfoliated WS_2 (gray) which is eliminated in the hybrid material **2** (black).

CONCLUSIONS

We successfully synthesized and characterized the covalently modified WS_2-pyrene hybrid material **2** based on the addition of pyrene-modified 1,2-dithiolane species on exfoliated WS_2. Then, the hybrid material **2** was employed in a proof-of-concept application as resistive photosensor, whose response was found to be linearly dependent on light intensity. There are a number of clear benefits that arise from the particular 1,2-dithiolane functionalization of WS_2. Firstly, the functionalisation improved the quality of the host nanoflake WS_2 material itself, largely restoring its WS_2 stoichiometry and reducing the number of vacancies, oxidation and other damage sites liable to impede photoelectric response. This reduction in damage sites also stabilises the material, and when coupled with a protective pyrene surface layer[41], reduces degradation and associated signal drift during irradiation. Secondly, the good solubility achieved for WS_2-pyrene hybrid material **2** allows simpler manipulation in wet media, making it suitable for device fabrication. Third, pyrene acts itself as an additional photoactive source, donating charge to the host WS_2 and increasing the photosensitivity of the sample by a factor of 2-3. The signal-to-power sensitivity was additionally enhanced. While previous WS_2 functionalization treatments have also demonstrated enhanced sensitivity this is generally at the expense of sensor reaction time, whereas in the current case the device reaction time is actually enhanced.

While this study serves as a proof-of-concept, there are many other photo-active species such as porphyrins, phthalocyanines or perylenes, which could be further explored in order to broaden the spectral range of optical absorption and further enhance charge transfer interactions with TMDs, particularly when employed in complementary combinations.

ASSOCIATED CONTENT

Supporting Information

The Supporting Information is available free of charge on the ACS Publications website.

AUTHOR INFORMATION

Corresponding Author

***E-mail:** tagmatar@eie.gr

Present Address

¶ Department of Chemistry, Nagoya University, Nagoya 464-8602, Japan.

Author Contributions

The authors declare no conflicts of interest.

ACKNOWLEDGMENT

This project has received funding from the European Union's Horizon 2020 research and innovation programme under the Marie Sklodowska-Curie grant agreement No 642742, under the "Graphene Flagship" project grant agreement No 881603 and under the "ESTEEM3" project grant agreement No 823717. Partial support of this work by the project "Advanced Materials and Devices" (MIS 5002409) which is implemented under the "Action for the Strategic Development on the Research and Technological Sector" funded by the Operational Program "Competitiveness, Entrepreneurship and Innovation" (NSRF 2014-2020) and co-

financed by Greece and the European Union (European Regional Development Fund) is also acknowledged. The HRSTEM and SR-EELS studies were conducted at the Laboratorio de Microscopias Avanzadas, Instituto de Nanociencia de Aragon, Universidad de Zaragoza, Spain. R.A. gratefully acknowledges the support from the Spanish Ministerio de Economia y Competitividad (MAT2016-79776-P), from the Government of Aragon and the European Social Fund under the project "Construyendo Europa desde Aragon" 2014-2020 (grant number E13_17R).

REFERENCES

1. Stephenson, T.; Li, Z.; Olsen, B.; Mitlin, D. Lithium Ion Battery Applications of Molybdenum Disulfide (MoS_2) Nanocomposites. *Energy Environ. Sci*. **2014**, *7*, 209−231.

2. Rowley-Neale, S.; Foster, C.; Smith, G.; Brownson, D.; Banks, C. E. Mass-Producible, 2D-$MoSe_2$ Bulk Modified Screen-Printed Electrodes Provide Significant Electrocatalytic Performances Towards the Hydrogen Evolution Reaction. *Sustainable Energy Fuels* **2017**, *1*, 74−83.

3. Perivoliotis, D. K.; Tagmatarchis, N. Recent Advancements in Metal-Based Hybrid Electrocatalysts Supported on Graphene and Related 2D Materials for the Oxygen Reduction Reaction. *Carbon* **2017**, *118*, 493−510.

4. Shanmugam, M.; Durcan, C. A.; Yu, B. Layered Semiconductor Molybdenum Dsulfide Nanomembrane Based Schottky-Barrier Solar Cells. *Nanoscale* **2012**, *4*, 7399−7405.

5. Pagona, G.; Bittencourt, C.; Arenal, R.; Tagmatarchis, N. Exfoliated Semiconducting Pure 2H-MoS_2 and 2H-WS_2 Assisted by Chlorosulfonic Acid. *Chem. Commun*. **2015**, *51*, 12950−12953.

6. Matte, H. S. S. R.; Gomathi, A.; Manna, A. K.; Late, D. J.; Datta, R.; Pati, S. K.; Rao, C. A. N. R. MoS_2 and WS_2 Analogues of Graphene. *Angew. Chem. Int. Ed*. **2010**, *49*, 4059−4062.

7. Zeng, Z.; Yin, Z.; Huang, X.; Li, H.; He, Q.; Lu, G.; Boey, F.; Zhang, H. Single-layer Semiconducting Nanosheets: High-Yield Preparation and Device Fabrication. *Angew. Chem. Int. Ed*. **2011**, *50*, 11093−11097.

8. Yang, D.; Frindt, R. F. Li-Intercalation and Exfoliation of WS_2. *J. Phys. Chem. Solids* **1996**, *57*, 1113−1116.

9. Shi, Y.; Li, H.; Li, L.-J. Recent Advances in Controlled Synthesis of Two-Dimensional Transition Metal Dichalcogenides via Vapour Deposition Techniques *Chem. Soc. Rev*. **2015**, *44*, 2744−2756.

10. Grayfer, E.D.; Kozlova, M.N.; Fedorov, V.E. Colloidal 2D Nanosheets of MoS_2 and Other Transition Metal Dichalcogenides Through Liquid-Phase Exfoliation. *Adv. Colloid Interface Sci*. **2017**, *245*, 40−61.

11. Canton-Vitoria, R.; Stangel, C.; Tagmatarchis, N. Electrostatic Association of Ammonium-Functionalized Layered-Transition-Metal Dichalcogenides With an Anionic Porphyrin, *ACS Appl. Mater. Interfaces* **2018**, *10*, 23476−23480.

12. Canton-Vitoria, R.; Vallan, L.; Urriolabeitia, E.; Benito, A. M.; Maser, W. K.; Tagmatarchis, N. Electronic Interactions in Illuminated Carbon Dot/MoS_2 Ensembles and Electrocatalytic Activity Towards Hydrogen Evolution, *Chem. Eur. J*. **2018**, *24*, 10468−10474.

13. Canton-Vitoria, R.; Istif, E.; Hernández-Ferrer, J.; Urriolabeitia, E. P.; Benito, A. M.; Maser, W. K.; Tagmatarchis, N. Integrating Water-Soluble Polythiophene With Transition Metal Dichalcogenides for Managing Photoinduced Processes. *ACS Appl. Mater. Interfaces* **2019**, *11*, 5947−5956.

14. Canton-Vitoria, R.; Sayed-Ahmad-Baraza, Y.; Pelaez-Fernandez, M.; Arenal, R.; Bittencourt, C.; Ewels, C. P.; Tagmatarchis, N. Functionalization of MoS_2 With 1,2-dithiolanes: Toward Donor-Acceptor Nanohybrids for Energy Conversion. *npj 2D Mater. Appl*. **2017**, *1*, 1−13.

15. Vallan, L.; Canton-Vitoria, R.; Gobeze, H. B.; Jang, Y.; Arenal, R.; Benito, A. M.; Maser, W. K.; D'Souza, F.; Tagmatarchis, N. Interfacing Transition Metal Dichalcogenides With Carbon Nanodots for Managing Photoinduced Energy and Charge-Transfer Processes. *J. Am. Chem. Soc*. **2018**, *140*, 13488−13496.

16. Canton-Vitoria, R.; Gobeze, H. B.; Blas-Ferrando, V. M.; Ortiz, J.; Jang, Y.; Fernández-Lázaro, F.; Sastre-Santos, Á.; Nakanishi, Y.; Shinohara, H.; D'Souza, F.; Tagmatarchis, N. Excited-State Charge Transfer in Covalently Functionalized MoS_2 With a Zinc Phthalocyanine Donor-Acceptor Hybrid. *Angew. Chem. Int. Ed*. **2019**, *58*, 5712−5717.

17. Canton-Vitoria, R.; Scharl, T.; Stergiou, A.; Cadranel, A.; Arenal, R.; Guldi, D. M.; Tagmatarchis, N. Ping-Pong Intercomponent Energy Transfer in Covalently Linked Porphyrin-MoS_2 Architectures. *Angew. Chem. Int. Ed*. **2020**, *59*, 3976-3981.

18. Chen, H.; Liu, H.; Zhang, Z.; Hu, K.; Fang, X. Nanostructured Photodetectors: From Ultraviolet to Terahertz. *Adv. Mater*. **2016**, *28*, 403-433.

19. Perea-López, N.; Elías, A.; Berkdemir, A.; Castro-Beltran, A.; Gutiérrez, H.; Feng, S.; Lv, R.; Hayashi, T.; López-Urías, F.; Ghosh, S.; Muchharla, B.; Talapatra, S.; Terrones, H.; Terrones, M. Photosensor Device Based on Few-Layered WS_2 Films. *Adv. Funct. Mater*. **2013**, *23*, 5511-5517.

20. Huang, Y.; Zhuge, F.; Hou, J.; Lv, L.; Luo, P.; Zhou, N.; Gan, L.; Zhai, T. Van der Waals Coupled Organic Molecules With Monolayer MoS2 For Fast Response Photodetectors With Gate-Tunable Responsivity. *ACS Nano* **2018**, *12*, 4062-4073.

21. Yin, Z.; Li, H.; Li, H.; Jiang, L.; Shi, Y.; Sun, Y.; Lu, G.; Zhang, Q.; Chen, X.; Zhang, H. Single-Layer Mos_2 Phototransistors. *ACS Nano* **2011**, *6*, 74-80.

22. Jo, S.; Ubrig, N.; Berger, H.; Kuzmenko, A. B.; Morpurgo, A. F. Mono- and Bilayer WS_2 Light-Emitting Transistors. *Nano Lett.* **2014**, *14*, 2019–2025.

23. Iqbal, M.; Iqbal, M.; Khan, M.; Shehzad, M.; Seo, Y.; Park, J.; Hwang, C.; Eom, J. High-Mobility and Air-Stable Single-Layer WS_2 Field-Effect Transistors Sandwiched Between Chemical Vapor Deposition-Grown Hexagonal BN Films. *Sci. Rep*. **2015**, *5*, 10699–10708.

24. Liu, L.; Kumar, S. B.; Ouyang, Y. Performance Limits of Monolayer Transition Metal Dichalcogenide Transistors. *IEEE Trans. Electron Dev*. **2011**, *58*, 3042–3047.

25. Fan, Y.; Zhou, Y.; Wang X. Photoinduced Schottky Barrier Lowering in 2D Monolayer WS_2 Photodetectors. *Adv. Opt. Mater.* **2016**, *4*, 1573–1581.

26. Perea-López, N.; Elías, A. L.; Berkdemir A. Photosensor Device Based on Few- Layered WS_2 Films. *Adv. Funct. Mater.* **2013**, *23*, 5511–5517.

27 Gao, J.; Li, B.; Tan, J.; Chow, P.; Lu, T.; Koratkar, N. Aging of Transition Metal Dichalcogenide Monolayers. *ACS Nano* **2016**, *10*, 2628-2635.

28. Leonhardt, A.; Chiappe, D.; Asselberghs, I.; Huyghebaert, C.; Radu, I.; De Gendt, S. Improving MOCVD MoS_2 Electrical Performance: Impact of Minimized Water and Air Exposure Conditions. *IEEE Electron Device Lett*. **2017**, *38*, 1606-1609.

29. Britnell, L.; Ribeiro, R.; Eckmann, A.; Jalil, R.; Belle, B.; Mishchenko, A.; Kim, Y.; Gorbachev, R.; Georgiou, T.; Morozov, S.; Grigorenko, A.; Geim, A.; Casiraghi, C.; Neto, A.; Novoselov, K. Strong Light-Matter Interactions in Heterostructures of Atomically Thin Films. Science **2013**, *340*, 1311-1314.

30. Liu, Y.; Huang, W.; Chen, W.; Wang, X.; Guo, J.; Tian, H.; Zhang, H.; Wang, Y.; Yu, B.; Ren, T.-L.; Xu, J. Plasmon Resonance Enhanced WS_2 Photodetector With Ultra-High Sensitivity and Stability. *App. Surf. Sci.* **2019**, 481, 1127–1132.

31. Zhang, C.; Wang, S.; Yang, L.; Liu, Y.; Xu, T.; Ning, Z.; Zak, A.; Zhang, Z.; Tenne, R.; Chen, Q. High-Performance Photodetectors for Visible and Near-Infrared Lights Based on Individual WS_2 Nanotubes. *App. Phys. Lett*. **2012**, *100*, 243101.

32. Lan, C.; Zhou, Z.; Zhou, Z.; Li, C.; Shu, L.; Shen, L.; Li, D.; Dong, R.; Yip, S.; Ho, J. Wafer-Scale Synthesis of Monolayer WS_2 for High-Performance Flexible Photodetectors by Enhanced Chemical Vapor Deposition. *Nano Research* **2018**, *11*, 3371-3384.

33. Li, H.; Huang, K.; Zhang, Y. Enhanced Photoresponsivity of the GOQDs Decorated WS_2 Photodetector. *Mater. Res. Express* **2019**, *6*, 045902.

34. Jia, Z.; Xiang, J.; Wen, F.; Yang, R.; Hao, C.; Liu, Z. Enhanced Photoresponse of SnSe-Nanocrystals-Decorated WS_2 Monolayer Phototransistor. *ACS Appl. Mater. Interfaces* **2016**, *8*, 4781-4788.

35.Jia, Z.; Xiang, J.; Mu, C.; Wen, F.; Yang, R.; Hao, C.; Liu, Z. Improved Photoresponse and Stable Photoswitching of Tungsten Disulfide Single-Layer Phototransistor Decorated With Black Phosphorus Nanosheets. *J. Mater. Sci.* **201**7, *52*, 11506-11512.

36. Huang, Y.; Zhuge, F.; Hou, J.; Lv, L.; Luo, P.; Zhou, N.; Gan, L.; Zhai, T. Van der Waals Coupled Organic Molecules With Monolayer MoS_2 for Fast Response Photodetectors With Gate-Tunable Responsivity. *ACS Nano* **2018**, *12*, 4062-4073.

37. Liu, A. C. Y.; Arenal, R.; Miller, D. J.; Chen, X.; Johnson, J. A.; Eryilmaz, O. L.; Erdemir, A.; Woodford, J.B., Structural Order in Near-Frictionless Hydrogenated Diamond Like Carbon Films Probed at Three Length Scales Via Transmission Electron Microscopy. *Phys. Rev. B* **2007**, *75*, 205402.

38. Arenal, R.; De Matteis, L.; Custardoy, L.; Mayoral, A.; Grazu, V.; de la Fuente, J. M.; Marquina, C.; Ibarra, M.R. Spatial-Resolved EELS Analyses of Antibody Distribution on Bio-Functionalized Magnetic Nanoparticles, *ACS Nano* **2013,** *7*, 4006-4013**.**

39. Arenal, R.; Lopez-Bezanilla, A. In Situ Formation of Carbon Nanotubes Encapsulated Within Boron Nitride Nanotubes Via Electron Irradiation, *ACS Nano* **2014,** *8*, 8419-8425**.**

40. Zhao, W.; Ghorannevis, Z.; Chu, L.; Toh, M.; Kloc, C.; Tan, P.; Eda, G. Evolution of Electronic Structure In Atomically Thin Sheets of WS_2 and WSe_2. *ACS Nano* **2012**, *7*, 791-797.

41 Canton-Vitoria, R.; Sayed-Ahmad-Baraza, Y.; Humbert, B.; Arenal, R.; Ewels, C.; Tagmatarchis, N. Pyrene Coating Transition Metal Disulfides as Protection From Photooxidation and Environmental Aging. *Nanomaterials* **2020**, *10*, 363.

TOC

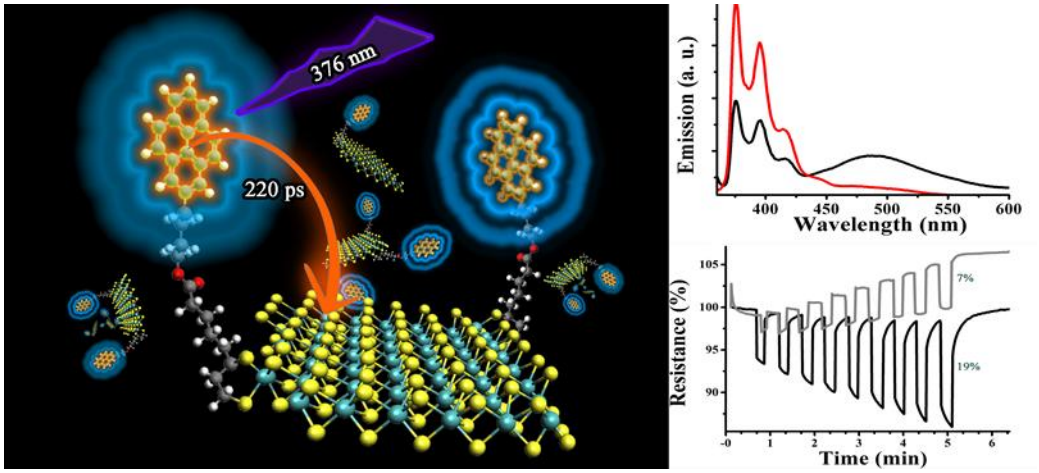
376 nm
220 ps
Emission (a. u.)
400
450
500
550
600
Wavelength (nm)
Resistance (%)
105
100
95
90
7%
19%
-0
1
2
3
4
5
6
Time (min)